Progress In Electromagnetics Research, Vol. 126, 101–120, 2012

DESIGN OF A DUALBAND OMNIDIRECTIONAL PLANAR MICROSTRIP ANTENNA ARRAY

K. P. Wei, Z. J. Zhang*, and Z. H. Feng

Department of Electronic Engineering, Tsinghua University, Beijing, China

Abstract—This paper proposes and designs a new method of dualband omnidirectional planar microstrip antenna array. A cascade of transposed microstrip lines have been adapted to produce effective antenna structures that radiate omnidirectionally, with high efficiency, low reflection, and useful radiation patterns. In this paper, the antenna structure has been found to have low-pass characteristics due to the periodic discontinuities at the transposed junctions. The analysis and design of the low-pass characteristic are performed according to the filter theory of periodic structures and full-wave simulation. Therefore, a relatively higher frequency radiating array is appropriately designed with a low-pass filtering attribute, which prevents the lower frequency radiators from resonating at the relatively higher frequency. An air gap between adjacent transposed sections is proposed in order to enhance impedance matching, and a fork shape stub at the end is used as a virtual short point to enhance radiation at the higher frequency. Finally a single port dualband omnidirectional antenna array is obtained by locating the higher frequency radiating array with low-pass filtering attribute near the antenna feed and a relatively lower frequency radiating array at the end. An example of a dualband omnidirectional planar array is demonstrated experimentally, which operates at $2.32 \sim 2.56\,\text{GHz}$ and $5.65 \sim 6.10\,\text{GHz}$ with $S_{11} < -10\,\text{dB}$ and a stable radiation pattern, and corresponding gains of $7.0 \sim 7.6\,\text{dBi}$ and $6.9 \sim 7.9\,\text{dBi}$ respectively.

Received 21 November 2011, Accepted 27 December 2011, Scheduled 9 March 2012

* Corresponding author: Zhijun Zhang (zjzh@tsinghua.edu.cn).

1. INTRODUCTION

Modern wireless communications systems typically require high-gain omnidirectional (in the azimuth plane) antennas to cover a large service area [1, 2]. In conventional applications, vertical dipole antennas with a half-wavelength resonant structure are the most popular choice. For many applications such as base stations or WLAN access-points (AP) [3–5], the half-wavelength dipole antenna has a gain of about 2.15 dBi, which may not be sufficient. Moreover, the natural standing wave current distribution on the resonant long wire antenna produces one radiation lobe for each half-wavelength antenna section [6–8]. It is one of the oldest antennas, and has been studied for over a century.

Several phase-reversed antenna configurations immune to this problem have been proposed for high-directivity in the elevation plane. The collinear array (CoA) of dipole antennas is a well-known candidate for increasing the gain of a single dipole. The original idea comes from Franklin [9]. He first designed CoA from a long wire that had $\lambda/4$ transverse narrow U-shaped sections to provide a phase shift to maintain in-phase feeding of the straight $\lambda/2$ parts of the longitudinal radiating wire antenna. In this antenna, the U-shaped sections maintain in-phase currents along the longitudinal axis, while the opposing and close transverse currents of the U-shaped sections cancel out to avoid cross-polar radiation. Based on Franklin antenna's concept, Wheeler designed an omnidirectional COCO (Colinear Coxial) antenna [10], made of a series of sections of solid-dielectric coaxial cable with their inner and outer conductors transposed at each junction. Since each section has an effective length of nearly 0.5 wavelengths, the whole array of cables appear to be in the same phase. The cylindrical patch [11] used to be adopted in order to solve the feeding problem, but the cost of constructing such a cylindrical array antenna is usually high, since the antennas had to conform to the cylindrical ground surface. Using a theory similar to that of the COCO antenna, Bancroft and Brennan further presented various microstrip variations [12–14] of the COCO antenna. These omnidirectional antennas have the advantages of planarity, easy integration and low construction costs, compared to coaxial antennas.

Due to the rapid development of mobile communications, the need for omnidirectional antennas with multi-band operation has increased considerably [15–17]. For instance, wireless local area network (WLAN) operates at both 2.4 to 2.5 GHz (IEEE 802.11b and IEEE 802.11g) and 5.15 to 5.875 GHz (IEEE 802.11a) frequency bands [18–20]. To integrate both bands into one device, for simple system configuration and cost reduction, it is important to develop dualband

omnidirectional antennas with high directivity. Unfortunately, since the existing series-fed omnidirectional planar antennas needed a 180° phase shift to excite all radiating elements in phase, the distance between adjacent sections should be a half-wavelength. The traditional omnidirectional planar antenna array typically has 2% of impedance bandwidth and 2.3% of pattern bandwidth [12]. Therefore, designing a dualband planar omnidirectional antenna with narrow beams is still a significant challenge. Existing dual omnidirectional planar antenna arrays [18–20] could not control the radiation aperture, and have problems with small limited gain due to the shunt-fed network. Recently, the integration of dualband antennas based on two elements and bandpass filters has been considered to be one of the best solutions for dual or multiband systems, which can be used for the suppression of unwanted harmonics of the antenna and in the improvement of reflection loss and the selectivity of the antenna [21–25]. Therefore, we propose a novel design method of the dualband omnidirectional planar microstrip antenna array. Using the methods based on filter theory, the radiation aperture of the dualband array can be controlled, allowing both lower frequency and higher frequency radiators to co-exist and operate independently.

2. DESIGN METHODOLOGY

The omnidirectional (in the azimuth plane) antenna arrays are more difficult to design compared to directional antenna arrays, because that the feeding networks should be strictly arranged with no distortion of omnidirectional patterns. Since the feeding networks reciprocally disturb the omnidirectional patterns, omnidrectional arrays operating at different bands that are mounted independently with discrete ports are unworkable. Therefore, a dualband omnidiretional antenna array with stable omnidirectional radiation pattern is preferred due to its simple system configuration and potential for cost reduction. The existing dualband omnidiretional planar element has been achieved by employing different modes of chamfered dipoles [18–20], which could not be readily arranged to form an array with a controlled radiation aperture. The major aim of this paper is to provide a method for designing a dualband omnidirectional planar antenna array with controlled radiation aperture.

Omnidirectional antenna arrays with high gain are usually collinear arrays (CoA), which are based on the in-phase feeding of radiating elements that lie in a straight line. The major advantages of this collinear arrangement is that it results in much lower coupling between elements and has a typically omnidirectional

radiation without degradation caused by the feeding network. Due to the shunt-fed configuration being limited by the element numbers and complex feeding network, a collinear series-fed configuration is chosen in this paper. In order to avoid disturbing the omnidirectional radiation patterns by the feeding networks, the single port dualband omnidirectional antenna array shown in Fig. 1 is obtained by locating the higher frequency radiating array with low-pass filtering attributes near the antenna feed, and a relatively lower frequency radiating array at the end. To meet the requirements of IEEE 802.11a/b/g wireless local area network (WLAN), a 2.4/5.8-GHz dualband omnidirectional planar antenna array is presented as an example.

As mentioned above, the major issue regarding the design is the arrangement of the feeding network and the isolation between the 2.4 GHz radiator and 5.8 GHz radiator for the suppression of unwanted radiation patterns. For allowing both the 2.4 GHz array and 5.8 GHz array to co-exist and operate independently with controlled radiation apertures, the idea of a microwave filter is applied in this structure. The 5.8 GHz array near the antenna feed is also designed as a microstrip filter with low-pass characteristics at the 2.4 GHz frequency band. The low-pass filtering attribute is used to prevent the 5.8 GHz radiator from resonating at the 2.4 GHz frequency band. This transmits power at the 2.4 GHz frequency band to the 2.4 GHz array at the end. Since the 5.8 GHz high-order mode resonates on the 2.4 GHz array, which will result in unwanted radiation patterns. As a result, the 5.8 GHz signal should mostly be radiated by the 5.8 GHz array. Therefore, the radiation of the 5.8 GHz signal at the 5.8 GHz radiator should be enhanced.

A series-fed planar antenna array made of a cascade of transposed microstrip line sections has been proposed in [12], which is one of the best solutions to produce an omnidirectional radiation pattern with high directivity. In this paper, periodically transposed microstrip lines have also been found to allow a low-pass characteristic due to the periodic discontinuities at transposed junctions. The analysis and

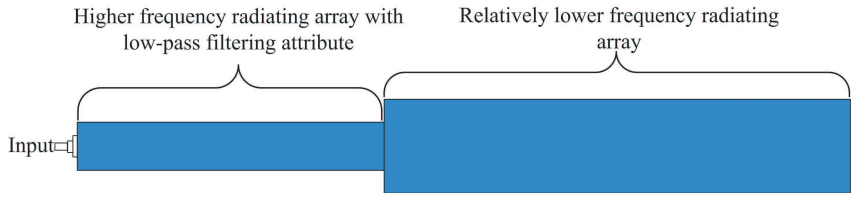

Figure 1. Schematic of the proposed single port dualband omnidirectional antenna array.

design of the low-pass characteristic are performed according to the filter theory of periodic structures explained in the next section.

3. LOW-PASS FILTERING ATTRIBUTES OF PERIODICALLY TRANSPOSED MICROSTRIP LINES

Figure 2 shows the overall configuration of periodically transposed microstrip lines. The structure is composed of a plurality of microstrip transmission line sections, periodically transposed at each junction with a period of d. The microstrip transmission line in this structure consists of two strip conductors of width w_1 and width w_2, which are separated by a dielectric material of permittivity ε_r and thickness h. All the microstrip transmission line sections have the same characteristic impedance of Z_c. Since the $(n-1)$th and nth microstrip transmission line sections are reversed, with the same dimensions, the small difference can be neglected in practice, so that the period of the structure can be considered to be equal to d.

As we can see, a transposed microstrip line section can be considered as a junction between a microstrip line and a converted microstrip line. Figs. 3(a), (b), and (c) show the electric and magnetic field distributions of the microstrip line, converted microstrip line and the transposed microstrip line sections respectively. It is clear that a discontinuity in a transposed junction is caused by an abrupt

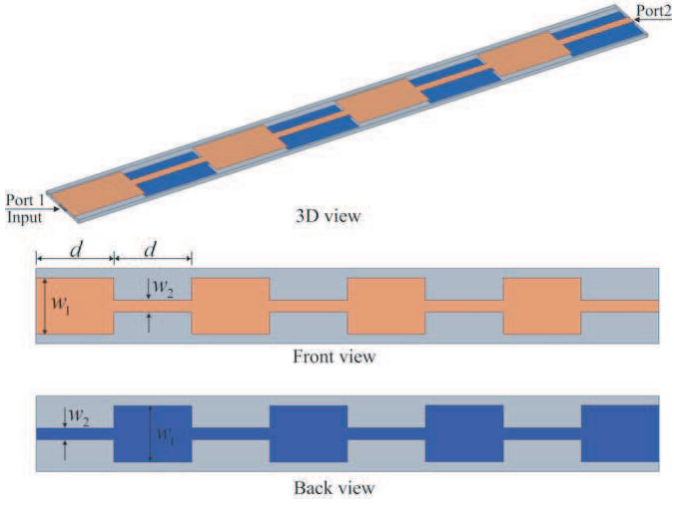

Figure 2. Overall configuration of periodically transposed microstrip line sections.

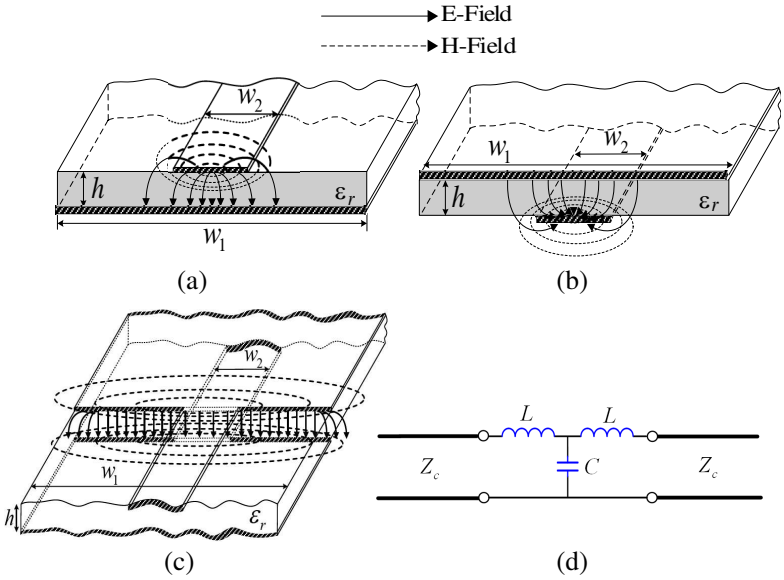

Figure 3. (a) Field distribution of microstrip line. (b) Field distribution of converted microstrip line. (c) Field distribution of transposed junction. (d) The discontinuity of transposed junction and its equivalent circuit.

change in the geometry of the strip conductor. Therefore, electric and magnetic field distributions are modified near the discontinuity. As shown in Figs. 3(a), (b), and (c), an abrupt alternation in the electric field distribution and magnetic field distribution occurs at the junction. Since the discontinuity dimensions are usually much smaller than the wavelength in the microstrip, it may be modeled by lumped element equivalent circuits. The altered electric field distribution gives rise to a change in capacitance, and the changed magnetic field distribution can be expressed in terms of an equivalent inductance. As shown in Fig. 3(d), the discontinuity of a transposed junction can be approximately represented as a T-equivalent circuit [26].

As we all know, periodic structures have passband and stopband characteristics similar to those of filters. To determine the frequency characteristics of the periodically transposed microstrip lines, the radiation resistances are neglected without affecting the propagation characteristics. Hence, the corresponding equivalent circuit model of the periodically transposed microstrip lines is shown in Fig. 4. If we consider the infinite line as being composed of a cascade of identical two-port networks, we can relate the voltages V and currents I on

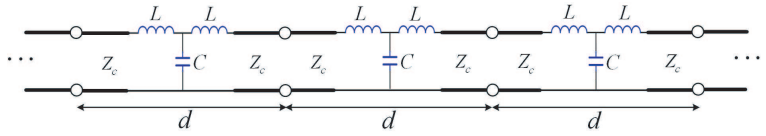

Figure 4. Equivalent circuit of the periodically transposed microstrip line sections shown in Fig. 1.

either side of the nth unit cell using the $ABCD$ matrix [27].

$$\begin{bmatrix} V_n \\ I_n \end{bmatrix} = \begin{bmatrix} A & B \\ C & D \end{bmatrix} \begin{bmatrix} V_{n+1} \\ I_{n+1} \end{bmatrix} = \begin{bmatrix} V_{n+1}e^{\gamma d} \\ I_{n+1}e^{\gamma d} \end{bmatrix} \tag{1}$$

Since $AD - BC = 1$

$$\cos \beta d = \frac{A + D}{2} \tag{2}$$

where A, B, C, and D are the matrix parameters for a cascade of a transmission line section of length $d/2$, a T-equivalent circuit and another transmission line section of length $d/2$.

$$\begin{bmatrix} A & B \\ C & D \end{bmatrix} = \begin{bmatrix} \cos\dfrac{\theta}{2} & jZ_c \sin\dfrac{\theta}{2} \\ \dfrac{j\sin\frac{\theta}{2}}{Z_c} & \cos\dfrac{\theta}{2} \end{bmatrix} \begin{bmatrix} 1-\omega^2 LC & j\omega L\left(2-\omega^2 LC\right) \\ j\omega C & 1-\omega^2 LC \end{bmatrix} \begin{bmatrix} \cos\dfrac{\theta}{2} & jZ_c \sin\dfrac{\theta}{2} \\ \dfrac{j\sin\frac{\theta}{2}}{Z_c} & \cos\dfrac{\theta}{2} \end{bmatrix} \tag{3}$$

where $\theta{=}kd$, and k is the propagation constant of the microstrip transmission line. Hence, the Equation (2) gives the following

$$\cos \beta d = \left(1 - \omega^2 LC\right) \cos kd - \left[\frac{\omega L\left(2 - \omega^2 LC\right)}{Z_c} + Z_c\, \omega C\right] \frac{\sin kd}{2} \tag{4}$$

Thus, depending on the frequency and the discontinuity, the periodically transposed microstrip lines will exhibit either passbands or stopbands, and therefore can be considered as a type of filer. To verify the filtering attribute of the periodically transposed microstrip lines, a simple prototype is analyzed with values for the parameters chosen to be $d = 16.5\,\text{mm}$, $w_1 = 8\text{mm}$, and $w_2 = 1.6\,\text{mm}$. It is designed on a low-cost teflon substrate with a dielectric constant $\varepsilon_r = 2.65$ and thickness $h = 0.8\,\text{mm}$. The T-equivalent circuit of the discontinuity of a transposed junction is $L = 1.82\,\text{nH}$ and $C = 1.08\,\text{pF}$, which is obtained from a full-wave parameter extracting technique. According to Equation (4), when the magnitude of the right-hand side is at unity

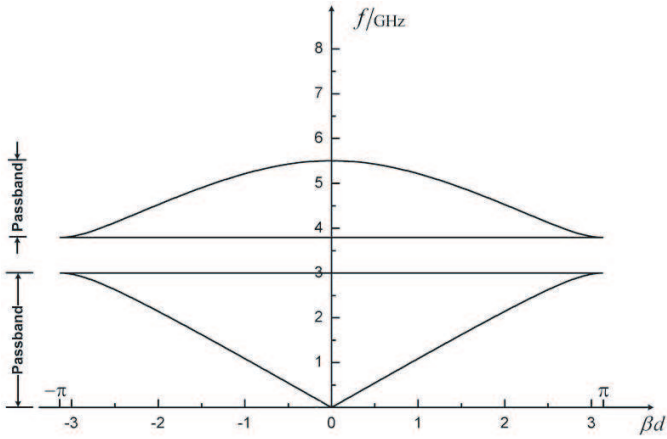

Figure 5. Filtering attribute of the periodically transposed microstrip line with the parameters chosen to be $d = 16.5\,\text{mm}$, $w_1 = 8\,\text{mm}$, and $w_2 = 1.6\,\text{mm}$ respectively. It is designed on a low-cost teflon substrate with a dielectric constant $\varepsilon_r = 2.65$ and thickness $h = 0.8\,\text{mm}$.

or lower, we have a passband, otherwise we have a stopband. Fig. 5 shows the f-k diagram for the first two passbands. It is clear that periodically transposed microstrip lines have low-pass characteristics. It can be designed as a microstrip filter with low-pass characteristics at the 2.4 GHz frequency band.

4. 5.8 GHZ OMNIDIRECTIONAL PLANAR ARRAY WITH LOW-PASS CHARACTERISTIC

As discussed in Section 3, due to the periodic discontinuities at transposed junctions, periodically transposed microstrip lines can be designed as a microstrip filter with low-pass characteristics at the 2.4 GHz frequency band. Employing the phase-reversal technique, the transposed microstrip line sections have converted the natural current distribution into a co-phased distribution of currents and radiated an omnidirectional pattern, when the period d is approximately equal to $\lambda_g/2$ at the 5.8 GHz frequency band. Based on the considerations above, an omnidirectional planar antenna array with a filtering attribute at 2.4 GHz and a radiating attribute at 5.8 GHz is designed and analyzed in this section. To investigate the attributes of the periodically transposed microstrip lines shown in Fig. 1, an eight-element ($N = 8$) antenna array was full-wave simulated using an Ansoft simulation software high frequency structure simulator (HFSS).

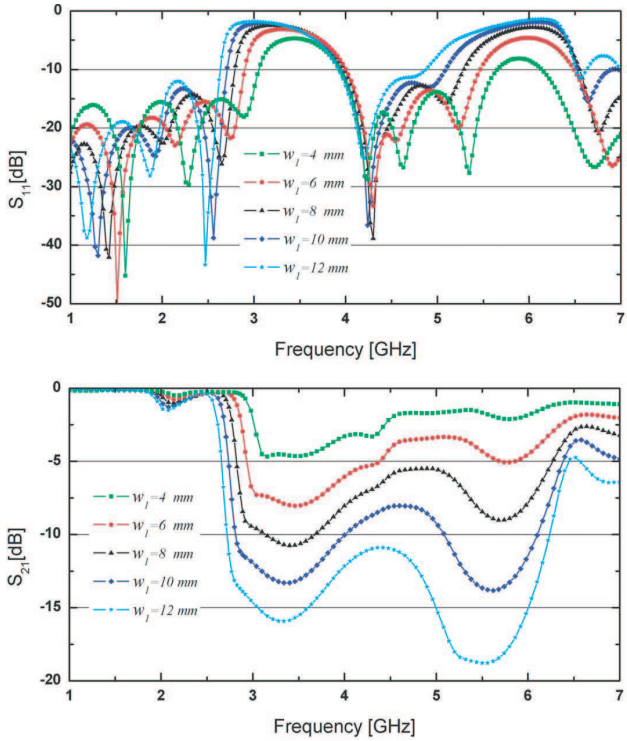

Figure 6. Simulated S-parameters for an eight-element antenna array consisting of transposed microstrip line sections proposed in Fig. 2, shown for various values of w_1. The other parameters are kept the same as in the prototype of Section 3.

4.1. Cutoff Frequency of the Low-pass Filter

To verify the low-pass characteristics analyzed in Section 3, the parameters of the array are kept the same as the prototype in Section 3. Based on the theory in Section 3, the cutoff frequency of the structure is determined by the period d and L, C in the T-equivalent circuit of the discontinuity. However, the period d should be fixed at 16.5 mm (approximately $\lambda_g/2$ at 5.8 GHz) to obtain a co-phased distribution of current. According to the discontinuities and model analysis, the element width w_1 is the key parameter to control the cutoff frequency of the low-pass filter. This is because the capacitance of C in the T-equivalent circuit caused by an abrupt change in field distribution, increases as the value of w_1 increases. It is confirmed by Fig. 6, which shows the S-parameters of the array versus frequency for various values

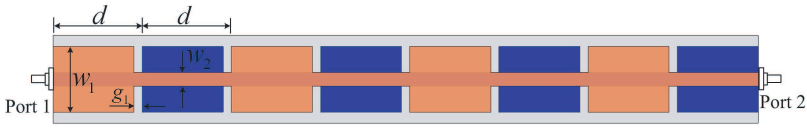

Figure 7. Geometry of an eight-element antenna array with an air gap between adjacent transposed sections.

of w_1. It shows that the full-wave simulation follows very well the analytical results of the filter theory in Section 3. This confirms the proposed structure which allows low-pass characteristics. It is also observed that the variation in w_1 is useful to tune the cutoff frequency. Moreover, the radiating attribute at the 5.8 GHz frequency band is also affected by the value of w_1. On the basis of comprehensive consideration, the value of w_1 is chosen to be 8 mm.

4.2. Impedance Matching at the 5.8 GHz Frequency Band

According to previous experiences of the previous series-fed arrays [14], the input impedance of the arrays are mainly determined by the element number N and the element width w_1. When the antenna is at resonance, we will designate the input impedance for the two elements ($N = 2$) as R_2. Equation (5) gives the input impedance of the array R_N as

$$R_N = \frac{2}{N} R_2 \tag{5}$$

where N is the total number of elements. As N increases, the input impedance of the array decreases rapidly away from the source impedance 50 Ω. Although narrowing the element width w_1 produces larger element impedance, the element width w_1 is fixed at 8 mm to obtain a low-pass attribute at the 2.4 GHz frequency band and a radiating attribute at the 5.8 GHz frequency band. Hence, an air gap between the adjacent transposed sections shown in Fig. 7 is proposed in order to enhance the impedance matching. Widening the air gap g_1 also produces larger element impedance. Therefore, the input impedance may be adjusted to 50 Ω by tuning the value of g_1. As shown in Fig. 8, a good impedance matching at a resonance of the 5.8 GHz frequency band is obtained at the air gap, $g_1 = 1.5$ mm.

4.3. Radiation Enhancement at the Frequency of 5.8 GHz

As mentioned in Section 2, the 5.8 GHz signal should mostly be radiated by the 5.8 GHz array and prevented from transmitting to the 2.4 GHz array at the end. This is because the 5.8 GHz high-order

mode resonance on the 2.4 GHz array will result in unwanted radiation patterns. In order to enhance the 5.8 GHz radiation, a fork shape stub, as shown in Fig. 9, is added. It works as a virtual short point at the 5.8 GHz frequency band to enhance radiation. Due to the fork shape stub being considered as a little shunt capacitance to the input port, there would be almost no influence on the impedance matching at the

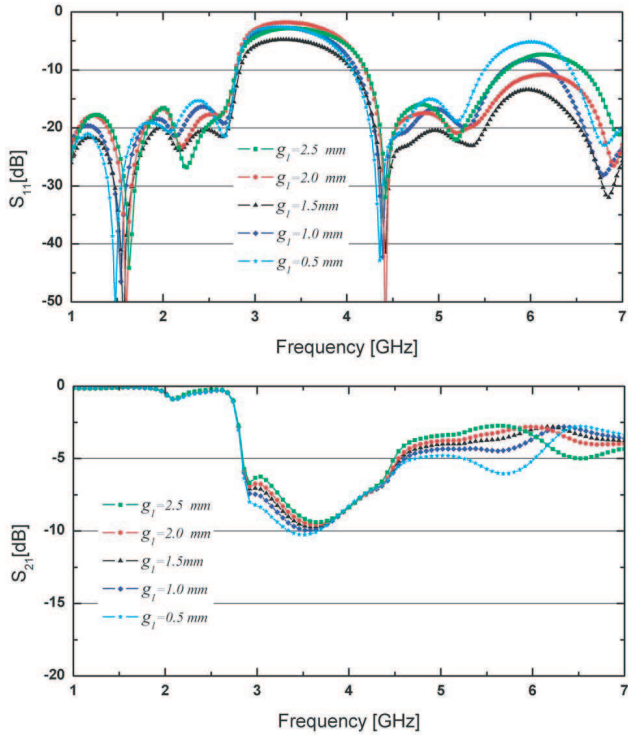

Figure 8. Simulated S-parameters for an eight-element antenna array with an air gap between the adjacent transposed sections, shown for various values of g_1 ($d = 16.5$ mm, $w_1 = 8$ mm, and $w_2 = 1.6$ mm, $h = 0.8$ mm and $\varepsilon_r = 2.65$).

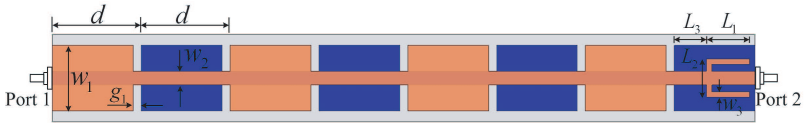

Figure 9. Geometry of the proposed 5.8 GHz antenna array with a fork shape stub.

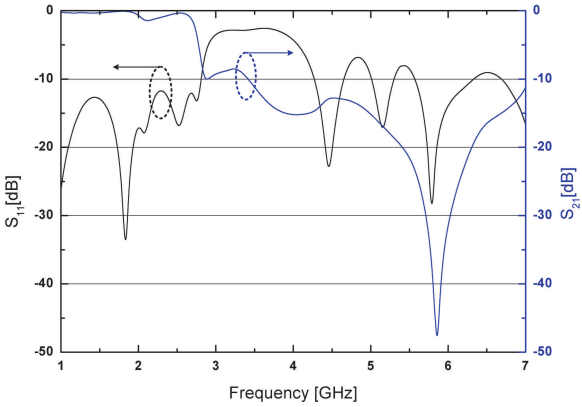

Figure 10. Simulated S-parameters for the proposed 5.8 GHz antenna array with a fork shape stub ($d = 16.5$ mm, $w_1 = 8$ mm, $w_2 = 1.6$ mm, $w_3 = 0.5$ mm, $g_1 = 1.5$ mm, $L_1 = 8$ mm $L_2 = 6$ mm, $L_3 = 6.25$ mm, $h = 0.8$ mm and $\varepsilon_r = 2.65$).

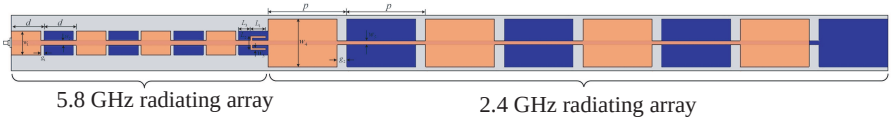

Figure 11. Overall configuration of the dualband omnidirectional planar microstrip antenna array.

2.4 GHz frequency band. As shown in Fig. 10, the low transmission coefficient S_{21} and reflection coefficient S_{11} from 5.6 GHz to 6.3 GHz indicate that the antenna has a higher radiation loss. The impedance matching at 2.4 GHz is still good, while a passband at 2.4 GHz is maintained. In the next Section this structure is implemented on a dualband omidirectional planar microstrip antenna array.

5. ANTENNA DESIGN OF THE DUALBAND OMNIDIRECTIONAL PLANAR MICROSTRIP ANTENNA ARRAY

Figure 11 shows the proposed dualband omnidirectional planar microstrip antenna array. The single port dualband omnidirectional antenna array consists of a 5.8 GHz radiating array with 2.4 GHz passband filtering attribute near the feed port, and a 2.4 GHz radiating array at the end. The 5.8 GHz omnidirectional planar array with a 2.4 GHz passband is discussed in Section 4. Similar to the design

of the 5.8 GHz radiating array, the 2.4 GHz omnidirectional planar array is achieved by designing the period p as being approximately equal to $\lambda_g/2$ at the 2.4 GHz frequency band. Optimized impedance matching at the 2.4 GHz frequency band can be obtained by adjusting the parameters of g_2, w_4 and w_5. The dualband omnidirectional planar microstrip antenna array shown in Fig. 11 was designed and simulated using Ansoft's HFSS full-wave simulator. The final design of the dualband omnidirectional array has the following parameters: $d = 16.5$ mm, $p = 40$ mm, $w_1 = 8$ mm, $w_2 = 1.6$ mm, $w_3 = 0.5$ mm, $w_4 = 16$ mm, $w_5 = 1.2$ mm, $g_1 = 1.5$ mm, $g_2 = 5$ mm, $L_1 = 8$ mm, $L_2 = 6$ mm and $L_3 = 6.25$ mm. The substrate of the proposed antenna array is low-cost telfon with a dielectric constant $\varepsilon_r = 2.65$ and a thickness $h = 0.8$ mm. The geometry of the overall antenna array is $445.5 \times 20 \times 0.8\,\text{mm}^3$.

To validate the design of the proposed dualband omnidirectional planar array intuitively, the simulated surface current vector distributions are also studied and the results are shown in Fig. 12. Fig. 12(a) depicts the vector current distribution at 2.45 GHz, which shows that the 5.8 GHz radiating array works as a microwave filter and transmits a 2.45 GHz signal to the 2.4 GHz radiating array at the end. All elements of 2.4 GHz radiating array are resonating in phase to obtain an omnidirection radiation pattern. Fig. 12(b) depicts the vector current distribution at 5.85 GHz. All elements of the 5.8 GHz radiating array are radiating in phase, while the 2.4 GHz radiators have a weak current distribution due to the effect of the fork shape stub. The discrete variations in the radiation aperture at the 2.4 GHz frequency band and the 5.8 GHz frequency band ensure stable radiation without grating lobes.

As shown in Fig. 13, a prototype of the proposed dualband array is built and tested to provide verification of the new design method. Fig. 14(a) shows the measured and simulated S_{11} of the constructed prototype. The measured data generally agrees with the simulated results obtained from the Ansoft simulation software high frequency structure simulator (HFSS). Only a slight upshifting is

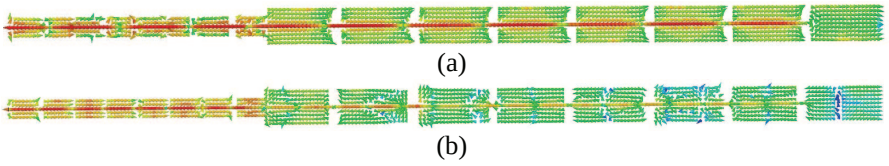

Figure 12. Simulated current vector distributions at (a) 2.45 GHz and (b) 5.85 GHz.

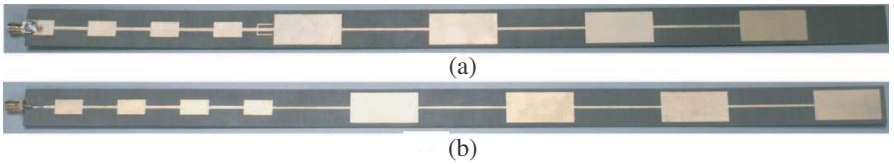

Figure 13. Photograph of the proposed antenna. (a) Front view. (b) Back view.

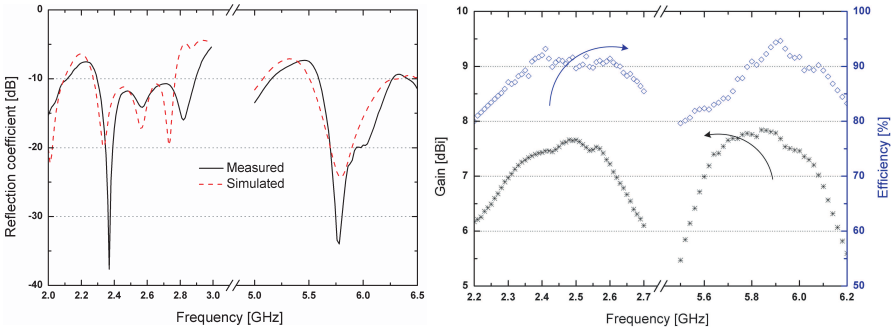

Figure 14. (a) Simulated and measured reflection coefficient values S_{11} of the proposed dualband omnidirectional planar array. (b) Measured antenna gain and efficiency of the proposed dualband omnidirectional planar array.

measured in the data for the 2.4 GHz and 5.8 GHz resonances compared to the simulated results. Note that a resonant mode is excited with good impedance matching at about 2.4 GHz, and the VSWR $2:1$ ($S_{11} < -10$ dB) impedance bandwidth is about 580 MHz (2.30–2.88 GHz). At about 5.8 GHz, a wide impedance bandwidth of about 680 MHz (5.59–6.27 GHz) is also obtained, which satisfies the required bandwidth of the wireless local area network (WLAN). Radiation characteristics of the proposed dualband array were also studied. An ETS 3-D chamber was used to measure the pattern of the fabricated prototype. The antenna measured gain and efficiency as a function of the operating frequency are presented in Fig. 14(b). The radiation pattern bandwidth of the high-gain omnidirectional (in the azimuth plane) antennas, which are defined as the frequency range over which the gain at the azimuth plane, is within 1 dB of its maximum gain. The measured pattern bandwidth is about 260 MHz (2.32–2.58 GHz) at the 2.4 GHz frequency band and about 450 MHz (5.65–6.10 GHz) at the 5.8 GHz frequency band. Across pattern bandwidth at 2.4 GHz, the

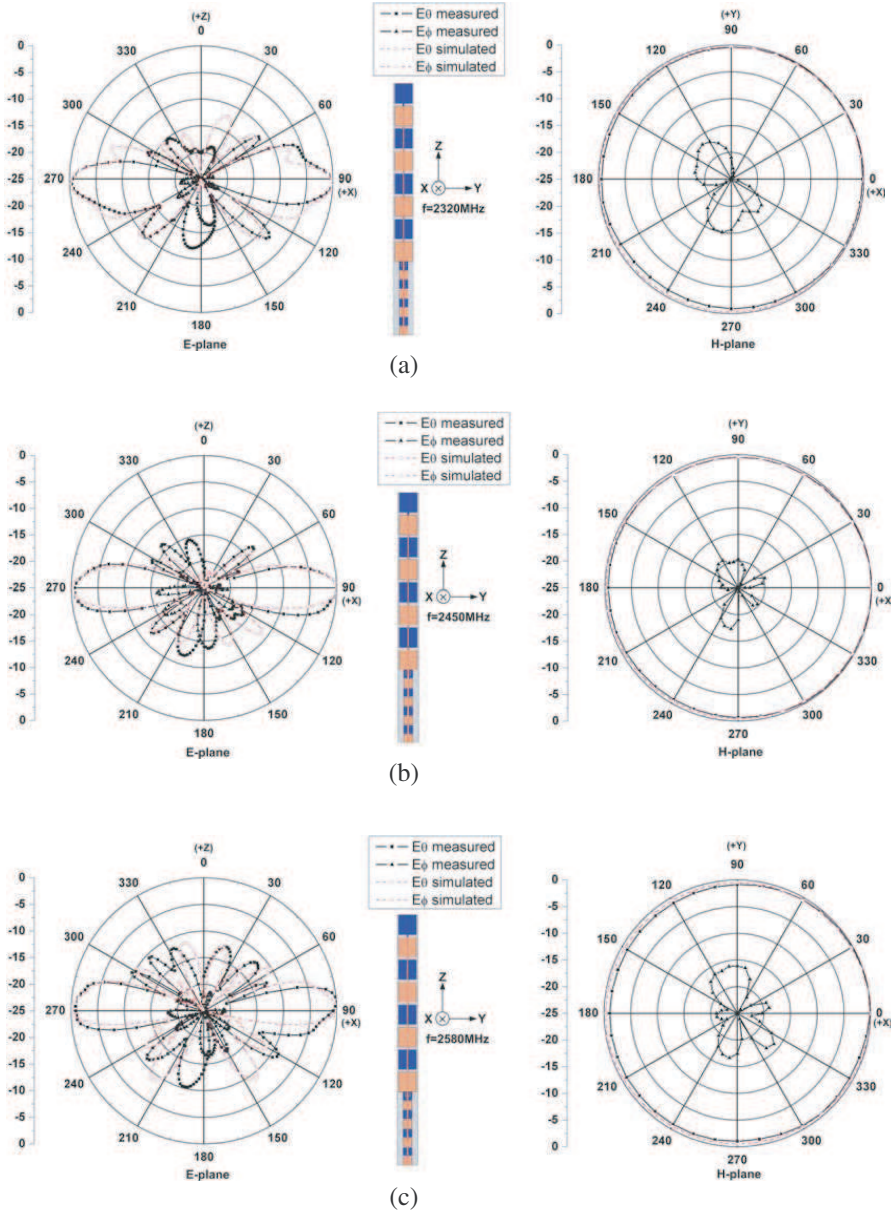

Figure 15. Measured normalized radiation patterns of the fabricated prototype in the pattern bandwidth at the 2.4 GHz frequency band. (a) $f = 2320$ MHz. (b) $f = 2450$ MHz. (c) $f = 2580$ MHz.

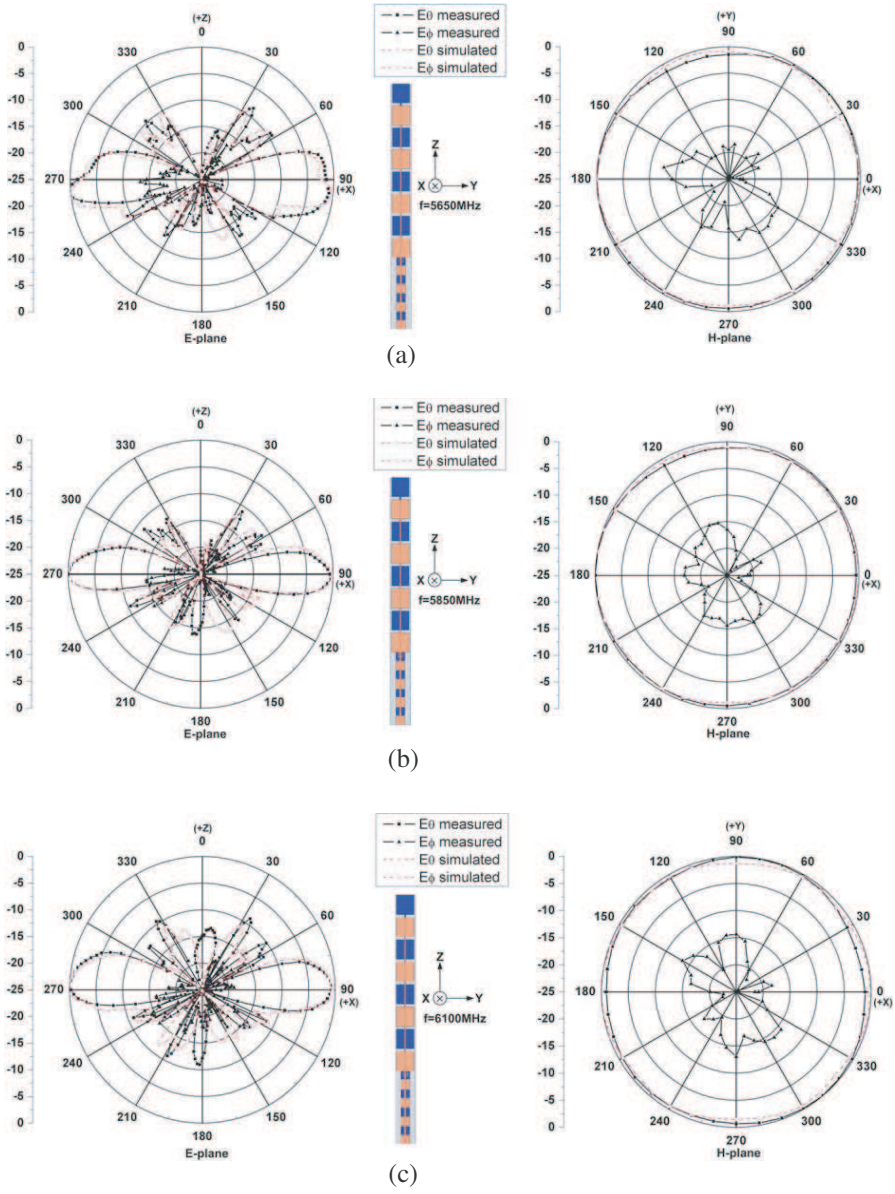

Figure 16. Measured normalized radiation patterns of the fabricated prototype in the pattern bandwidth at the 5.8 GHz frequency band. (a) $f = 5650$ MHz. (b) $f = 5850$ MHz. (c) $f = 6100$ MHz.

measured antenna gain is in a range of about $7.0 \sim 7.6$ dBi. At about 5.8 GHz, the measured antenna gain is $6.9 \sim 7.9$ dBi. It is clear that the radiation aperture of the dualband array is controlled. The ETS 3-D chamber can also provide an estimated value of the radiation efficiency of the measured antenna. The efficiency is defined as the ratio of radiated power versus the total available from the power source. Thus the efficiency value includes all impacts from mismatch loss, dielectric loss, conductor loss and matching component loss. The efficiency of the planar dipole array antenna varies from 87% to 93% in the pattern bandwidth at the 2.4 GHz frequency band, while it varies between 84% to 95% at the 5.8 GHz frequency band.

The measured normalized radiation patterns of the fabricated prototype in the pattern bandwidth at the 2.4 GHz frequency band are shown in Fig. 15. Only three representative frequencies ($f = 2.32$ GHz, $f = 2.45$ GHz and $f = 2.58$ GHz) are presented. Measurements at other operating frequencies across the 2.4 GHz band (not shown here for brevity) also show similar radiation patterns as those plotted here, which indicates that the radiation patterns are stable in the desired operating band. The measured normalized E-plane pattern and H-plane pattern of the fabricated prototype in the pattern bandwidth at the 2.4 GHz frequency band are also presented in Fig. 16. As can be seen from all the radiation patterns, the main beam is approximately fixed at broadside. From these results, it is clear that good omnidirectional radiation with vertical polarization in the H-plane (x-y plane) with a small gain variation of less than 1.5 dBi is obtained. In the E-plane (x-z plane), the HBPW (half-power beamwidth) of the proposed dualband planar array is about 19° at 2.45 GHz and 18° at 5.85 GHz.

6. CONCLUSION

A novel dualband omnidirectional planar microstrip antenna array with stable radiation pattern and gain has been studied and designed. In contrast with previous planar dualband antennas, this methodology for designing a higher frequency radiating array with a low-pass filtering attribute has been used to prevent the relatively lower frequency radiators from resonating at higher frequencies. Using a method based on filter theory, the radiation aperture of the dualband array is controlled, allowing both lower frequency and higher frequency radiators to co-exist and operate independently. A cascade of transposed sections of planar microstrip has been design to radiate at a higher frequency with a low-pass filtering attribute. The analysis and explanation of the low-pass characteristic are performed

according to the filter theory of periodic structures and by full-wave simulation. Finally, a single port dualband omnidirectional antenna array is obtained by locating the higher frequency radiating array with the low-pass filtering attribute near the antenna feed and a relatively lower frequency radiating array at the end. To meet the requirements of the IEEE 802.11a/b/g wireless local area network (WLAN), a simple prototype follows the design that has been demonstrated experimentally, which operates at $2.32 \sim 2.56$ GHz and $5.65 \sim 6.10$ GHz with $S_{11} < -10$ dB and a stable radiation pattern, and with corresponding gains of $7.0 \sim 7.6$ dBi and $6.9 \sim 7.9$ dBi respectively. Good vertically polarized omnidirectional radiation in the H-plane (x-y plane) with a small gain variation of less than 1.5 dBi is obtained.

ACKNOWLEDGMENT

This work is supported by the National Basic Research Program of China under Contract 2010CB327400, in part by the National Natural Science Foundation of China under Contract 60771009, the National High Technology Research and Development Program of China (863 Program) under Contract 2009AA011503, the National Science and Technology Major Project of the Ministry of Science and Technology of China 2010ZX03007-001-01, and Tsinghua-QUALCOMM associated Research Plan.

REFERENCES

1. Li, J. Y., J. L. Guo, Y. B. Gan, and Q. Z. Liu, "The tri-band performance of sleeve dipole antenna," *Journal of Electromagnetic Waves and Applications*, Vol. 19, No. 15, 2081–2092, 2005.
2. Khaleghi, A., "Diversity techniques with parallel dipole antennas: Radiation pattern analysis," *Progress In Electromagnetics Research*, Vol. 64, 23–42, 2006.
3. Zaker, R., C. Ghobadi, and J. Nourinia, "A modified microstrip-FED two-step tapered monopole antenna for UWB and WLAN applications," *Progress In Electromagnetics Research*, Vol. 77, 137–148, 2007.
4. Jaw, J.-L., F.-S. Chen, and D.-F. Chen, "Compact dualband CPW-fed slotted patch antenna for 2.4/5 GHz WLAN operation," *Journal of Electromagnetic Waves and Applications*, Vol. 23, No. 14–15, 1947–1955, 2009.

5. Panda, J. R. and R. S. Kshetrimayum, "A printed 2.4 GHz/5.8 GHz dual-band monopole antenna with a protruding stub in the ground plane for WLAN and RFID applications," *Progress In Electromagnetics Research*, Vol. 117, 425–434, 2011.
6. Franklin, C. S., "Improvements in wireless telegraph and telephone aerials," British Patent, No. 242, 342, 1924.
7. Ghosh, S., A. Chakraborty, and S. Sanyal, "Loaded wire antenna as EMI sensor," *Progress In Electromagnetics Research*, Vol. 54, 19–36, 2005.
8. Poljak, D. and V. Doric, "Wire antenna model for transient analysis of simple grounding systems. Part I: The vertical grounding electrode," *Progress In Electromagnetics Research*, Vol. 64, 149–166, 2006.
9. Solbach, K., "Microstrip-franklin antenna," *IEEE Trans. Antennas Propagat.*, Vol. 30, No. 4, 773–775, 1982.
10. Judasz, T. J. and B. B. Balsley, "Improved theoretical and experimental models for the coaxial colinear antenna," *IEEE Trans. Antennas Propagat.*, Vol. 37, 289–296, 1989.
11. Herscovici, N., Z. Sipus, and P.-S. Kildal, "The cylindrical omnidirectional patch antenna," *IEEE Trans. Antennas Propagat.*, Vol. 49, 1746–1753, Dec. 2001.
12. Bancroft, R. and B. Bateman, "An omnidirectional microstrip antenna," *IEEE Trans. Antennas Propagat.*, Vol. 52, 3151–3153, Nov. 2004.
13. Bancroft, R. and B. Bateman, "An omnidirectional planar microstrip antenna with low sidelobes," *Microwave and Optical Technology Letters*, Vol. 42, 68–69, Jul. 2004.
14. Bancroft, R., "Design parameters of an omnidirectional planar microstrip antenna," *Microwave and Optical Technology Letters*, Vol. 47, No. 5, 414–418, Dec. 2005.
15. Li, J.-Y. and Y.-B. Gan, "Multi-band characteristic of open sleeve antenna," *Progress In Electromagnetics Research*, Vol. 58, 135–148, 2006.
16. Wei, K., Z. Zhang, W. Chen, and Z. Fengm, and M. F. Iskander, "A triband shunt-fed omnidirectional planar dipole array," *IEEE Antennas Wireless Propag. Lett*, Vol. 9, 850–85, 2010.
17. Alkanhal, M. A. S., "Composite compact triple-band microstrip antennas," *Progress In Electromagnetics Research*, Vol. 93, 221–236, 2009.
18. Tze-Meng, O., K. G. Tan, and A. W. Reza, "A dual-band omnidirectional microstrip antenna," *Progress In Electromagnetics*

Research, Vol. 106, 363–376, 2010.

19. Si, L.-M. and X. Lv, "CPW-FED multi-band omni-directional planar microstrip antenna using composite metamaterial resonators for wireless communications," *Progress In Electromagnetics Research*, Vol. 83, 133–146, 2008.
20. Wu, Y.-J., B.-H. Sun, J.-F. Li, and Q.-Z. Liu, "Triple-band omni-directional antenna for WLAN application," *Progress In Electromagnetics Research*, Vol. 76, 477–484, 2007.
21. Shum, Y. H., K. M. Luk, and C. H. Chan, "Multi-band base station antenna with compact microstrip resonant cell filters," *IEE Proc. - Microw. Antennas Propag.*, Vol. 151, No. 6, 2004.
22. Suh, Y. H. and K. Chang, "A high-efficiency dual-frequency rectenna for 2.45-and 5.8-GHz wireless power transmission," *IEEE Trans. Microwave Theory Tech.*, Vol. 50, No. 7, 2002.
23. Barbarino, S. and F. Consoli, "UWB circular slot antenna provided with an inverted-l notch filter for the 5 GHz WLAN band," *Progress In Electromagnetics Research*, Vol. 104, 1–13, 2010.
24. Toh, W. K., X. M. Qing, and Z. N. Chen, "A planar dualband antenna array," *IEEE Trans. Antennas Propagat.*, Vol. 59, No. 3, 833–838, Mar. 2011.
25. Isom, R., M. F. Iskander, Z. Yun, and Z. Zhang, "Design and development of multiband coaxial continuous transerse stub (CTS) antenna arrays," *IEEE Trans. Antennas Propagat.*, Vol. 52, No. 8, Aug. 2004.
26. Gupta, K. C., R. Garg, and I. J. Bahl, *Microstrip Lines and Slotlines*, Artech House, Dedham, Mass., 1979.
27. Pozar, D. M., *Microwave Engineering*, 3rd edition, John Wiley & Sons, Inc., New York, 2005.